# Soil Salt Content Inversion Using Novel Salinity Indices Based on a Stacking Model

Yufei Lan[1], Ruiyin Tang[1,2*], Guohong Li[1,2], Xuqing Li[1,2], Yancang Wang[1,2], Haizhou Chen[1], Tingxuan Wang[1]

[1]North China Institute of Aerospace Engineering School of Remote Sensing and Information Engineering, Langfang 065000-

[2]Hebei Province Collaborative Innovation Center for Space Remote Sensing Information Processing and Application, Langfang 065000-

*852561856@qq.com

***Abstract*:** *Soil salinization poses a significant and escalating threat to agricultural productivity and ecological stability, affecting approximately one billion hectares globally and 76 million in China. This issue is particularly acute in the Coastal Areas of China, a vital region encompassing Tangshan, Cangzhou, and Qinhuangdao, where the interplay of coastal geography and intensive agriculture exacerbates salinity. Traditional monitoring via field sampling is labor-intensive and spatially sparse, proving inadequate for effective large-scale assessment. While remote sensing offers a powerful alternative, existing salinity indices, such as S1 and SI1, often fail in this region. Their performance is typically confounded by high vegetation cover and variable soil moisture, leading to low correlation with ground-truth data and limiting their predictive accuracy.To address these limitations, this study proposes four novel three-band salinity indices derived from Sentinel-2 multispectral imagery, engineered to enhance spectral sensitivity to salinity while minimizing distortions from vegetation and moisture. The development and validation of these indices were grounded in 95 in-situ soil electrical conductivity (EC) measurements collected in 2025. Subsequently, a Stacking ensemble regression model, integrating Multilayer Perceptron (MLP), Random Forest (RF), and XGBoost as base learners, was developed to quantify the relationship between the proposed spectral indices and measured soil EC.The results confirm the superiority of the novel indices. The best-performing index achieved a maximum Pearson correlation coefficient of 0.60 with soil EC, a substantial improvement over the 0.41 from the most effective existing index. The Stacking model yielded an outstanding validation coefficient of determination ($R^2$) of 0.870. This performance not only surpassed that of high-performing individual models like RF ($R^2$=0.773) and XGBoost ($R^2$=0.768), but also substantially exceeded the traditional Partial Least Squares Regression (PLSR) model ($R^2$=0.526). The success of the Stacking model highlights its ability to effectively fuse the predictive strengths of its diverse base learners, enhancing overall robustness and accuracy. This research presents a robust methodology for regional soil salinity estimation, providing critical decision-making support for sustainable land management in the China Coastal Areas and other similar salt-affected regions globally.*

*Keywords: Indices constructions, Machine Learning, Sentinel-2, Soil salinity, Stacking Regression*

## Introduction

Soil salinization is currently one of the biggest environmental problems of the 21st century, serving as the main cause of land degradation and desertification and threatening global food security and environmental sustainability. Soil salinization is defined as the excessive

accumulation of water-soluble salts present in the soil profile, especially sodium chloride (NaCl) (Abbas & Khan, 2007). It has been estimated that about 1 billion hectares of land are affected by salinization worldwide (FAO, 2021). In China, 76 million hectares of land are affected by salinization, accounting for about 6% of the total arable land. The gradual accumulation of salts increases the osmotic pressure of the soil, which significantly hinders the ability of roots of plants to uptake water and other nutrients from the soil. This physiological stress further affects the metabolism of plants, resulting in restricted growth of crops and ultimately leading to un reversible losses in agricultural yield. The magnitude of the problem makes it necessary to overcome the limitations of traditional measurement methods and develop large-scale, accurate monitoring technologies for this problem. Obtaining large-scale, high-precision information on the soil salt content is a necessary prerequisite for taking effective remediation measures to restore land productivity and agricultural sustainable development in the affected areas (Ma et al., 2024).

Until now, the assessment of soil salinization has mainly been based on direct in-situ measurements by extracting the electrical conductivity (EC) of the saturated soil extract in the laboratory (Hu et al., 2019). Although this method can provide highly accurate results for specific samples, it is laborious, time-consuming and resource consuming. In addition, its point-based characteristics can only provide scattered data, and it is unable to reflect the continuous spatial variation of soil salinity, which is obviously insufficient for the dynamic and large-scale monitoring required for effective regional land management.

The emergence of remote sensing in the last few decades can be considered as a revolution, an alternative and powerful tool for the monitoring of soil salinity. Remote sensing acquires information on electromagnetic energy reflected or emitted from the Earth's surface to estimate the topsoil salt content on a synoptic, non-destructive and fast way over large areas. The success of remote sensing for soil properties mapping has been limited in the past by sensor technology. Traditional multispectral sensors, like the Landsat Thematic Mapper (TM), have relatively broad spectral bands (100 - 200 nm) with insufficient spectral resolution to separate the weak and diagnostic absorption features of salt-affected soils and, as a result, they have not been suitable for accurate and precise mapping of soil properties (Davis et al., 2019). Recently, the launch of high-resolution multispectral sensors, like the European Space Agency's Sentinel satellite constellation, have opened new horizons for quantitative soil salinity remote sensing (Liang et al., 2024). In particular, the MultiSpectral Instrument (MSI) onboard the Sentinel-2 satellites provide data in 13 spectral bands, with improved resolution in the visible, near-infrared (NIR) and short-wave infrared (SWIR)

regions that have been found to be sensitive to changes in soil salinity variations (Konstantin Ivushkin et al., 2016). This provides a new opportunity to obtain information about the salinity of the objects in the satellite images with an increased accuracy (Jia et al., 2024).

To exploit the information content of data from modern sensors, numerous “generic” spectral soil salinity indices have been developed, which aim to increase the signal of the spectral information related to the soil salinity, such as the Soil Adjusted Vegetation Index (SAVI) (Dehni & Lounis, 2012), Normalized Difference Salinity Index (NDSI) (Nguyen et al., 2020) and Salinity Index (SI) (Nguyen et al., 2020). The main disadvantage of these “generic” indices is that they are developed for specific conditions of landscape and climate and may be ineffective when applied to new areas with different characteristics. In the China Coastal Areas, due to the high water table, the frequent occurrence of seawater intrusion and varying soil moisture, the factors affecting the reflectance are intertwined, and the signal of salt is often accompanied by other environmental variables. As a result, the known indices show a low correlation with the actual soil salinity in the coastal area, which hinders the construction of reliable predictive models.

Concurrently, the field has seen a rapid adoption of machine learning algorithms—including Support Vector Machines (SVM), Artificial Neural Networks (ANN), and Random Forest (RF)—which excel at modeling the complex, non-linear relationships between spectral data and soil properties(Boudibi et al., 2021; Wang et al., 2021). A significant challenge, however, is that the performance of these models is highly contingent on the availability of large, high-quality training datasets. In soil science, the acquisition of extensive ground-truth data is often prohibitively expensive and logistically challenging, leading to a persistent "small-sample" problem. Training a powerful model on weak features derived from ineffective indices with a limited dataset creates a high risk of overfitting, where the model learns spurious correlations from the training data and fails to generalize to new, unseen data. To overcome this, ensemble learning techniques like XGBoost and Stacking have emerged as state-of-the-art strategies(Dong & Tian, 2024; Zarei et al., 2021). By intelligently combining multiple base models, these methods can enhance stability and generalization performance, even under small-sample conditions.

This study posits that a high-accuracy soil salinity inversion framework requires a dual strategy: first, the engineering of novel, context-specific spectral features that are robust to local environmental conditions, and second, the application of an advanced model architecture designed to maximize generalization and stability with limited data. Based on this premise, this research aims to develop and validate a high-precision, high-robustness

soil salinity inversion method by synergistically combining innovative feature engineering with state-of-the-art ensemble learning. The specific objectives are: (a)To construct novel three-band soil salinity indices using Sentinel-2 data and systematically evaluate their performance against 17 widely used existing indices to demonstrate their superiority in the study area.(b)To develop and implement a Stacking ensemble model that integrates the predictive capabilities of Multilayer Perceptron (MLP), Random Forest (RF), and XGBoost to improve prediction accuracy and robustness, thereby addressing the small-sample challenge.(c)To apply the optimized model to Sentinel-2 imagery to generate a high-resolution soil salinity distribution map for the China Coastal Areas and to analyze the spatial patterns and underlying environmental drivers.

This research contributes a novel and validated methodological framework that offers a significant improvement in soil salinity monitoring accuracy for complex coastal regions. The findings provide critical technical support for precision agriculture and sustainable land management and are potentially transferable to other regions facing similar environmental challenges.

**Data Acquisition and Preprocessing**

**1. Study Area**

This study was carried out in the China Coastal Areas, which is a typical coastal saline-alkali area in China, located in parts of the municipalities of Tangshan, Cangzhou and Qinhuangdao. The study area is situated between 38°16′ and 39°55′ N latitude and 117°20′ and 119°51′ E longitude and covers about 4,874 km² in total area as shown in Figure 1.

The study area is characterized by flat terrain, high groundwater level and poor natural run off conditions. Under the influence of periodic seawater intrusion and mixing of riverine and marine water, the soils are generally severely and extensively affected by soil salinization. The majority of the land use is agriculture, with the main crops being wheat, maize and rice. It is well known that this area is an important agricultural production region in China. Thus, a thorough study on the soil salinity is essential for sustainable agricultural development.

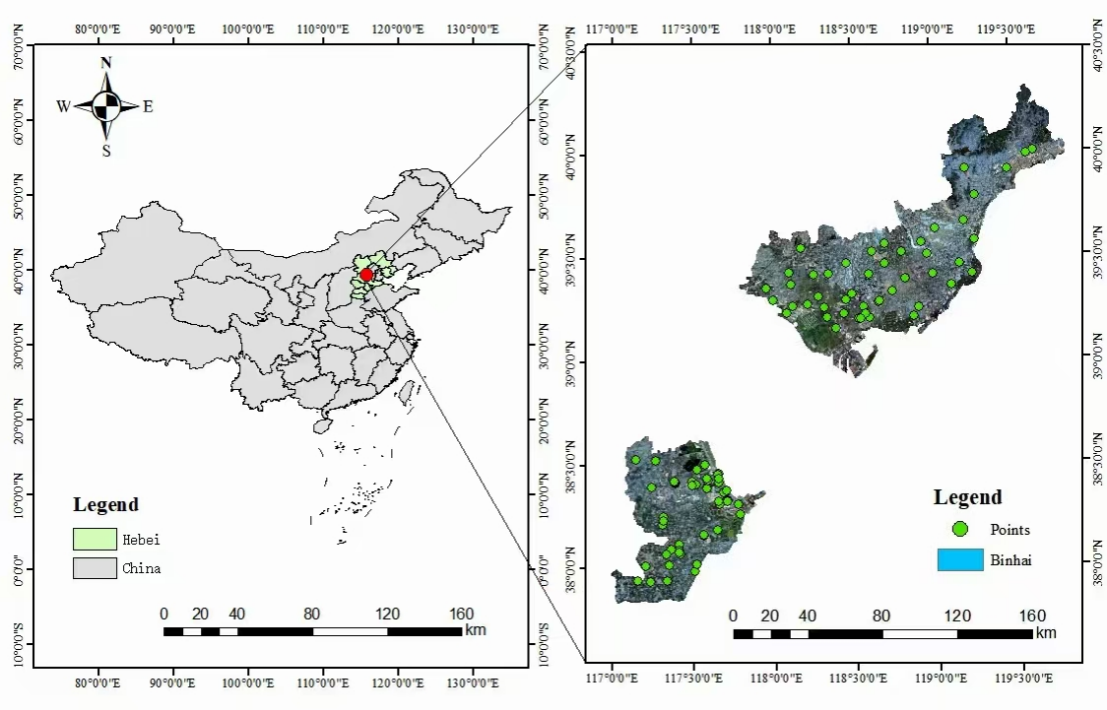


Figure 1: Overview of the study area.

## 2. Remote Sensing Data

The remote sensing data used in this study consisted of Sentinel-2 Level-2A (L2A) multispectral images acquired between March 16 and March 19, 2025, provided by the European Space Agency (ESA). The Sentinel-2A/B satellites are equipped with the MultiSpectral Instrument (MSI), which captures data in 13 spectral bands at spatial resolutions of 10 m, 20 m, and 60 m(Sabyasachi Kabiraj et al., 2023). This study focused on six bands that are particularly sensitive to soil properties and salinity (Table 1): Blue (B2, 490 nm), Green (B3, 560 nm), Red (B4, 665 nm), Near-Infrared (NIR, B8, 842 nm), Short-Wave Infrared 1 (SWIR 1, B11, 1610 nm) and Short-Wave Infrared 2 (SWIR 2, B12, 2190 nm). The L2A products are pre-processed for radiometric calibration and atmospheric correction, providing surface reflectance data. Further ortho-rectification was performed to ensure high geometric accuracy.

Table 1:Technical specifications and parameters of the Sentinel-2A/B satellite MultiSpectral Instrument.

| Technical specification | | Parameter |
|---|---|---|
| Spectral band | B2（Blue） | 490 nm |
| | B3（Green） | 560 nm |
| | B4（Red） | 665 nm |
| | B8（NIR） | 842 nm |
| | B11(SWIR 1) | 1610 nm |

| | | |
|---|---|---|
| | B12(SWIR 2) | 2190 nm |
| Satellite data | Width of cloth | 10/20/60 m |
| | Spatial resolution | 290 km |
| | Return cycle | 10 days |

**3. Field Sampling and Laboratory Analysis**

A field campaign for soil sample collection was conducted in mid-March 2025, strategically synchronized with the satellite overpass dates to minimize discrepancies arising from temporal changes in soil moisture or surface conditions. A total of 95 sampling points were established across the study area using a random sampling strategy to ensure representative coverage of different salinity levels and soil types. At each point, soil samples were collected from the topsoil layer (0-20 cm depth) using a soil auger, and the precise geographic coordinates were recorded with a GPS device. The collected samples were transported to the laboratory, where they were air-dried, ground, and passed through a sieve. Subsequently, the electrical conductivity (EC) of each sample was measured using standard laboratory procedures. These measurement results were converted into total salt content and became the ground-truth data used for model training and validation.

**Methodology**

**1. Methodological Workflow**

The overall technical workflow for soil salinity inversion is illustrated in Figure 2 and comprises four main steps:

(a) Data Preparation and Preprocessing: This stage involved the acquisition and preprocessing of Sentinel-2 L2A imagery and the collection and laboratory analysis of field soil samples to determine EC values. The preprocessed remote sensing images were then spatially matched with the ground sampling points to extract the corresponding surface reflectance values for each spectral band, creating the foundational dataset for the analysis.

(b) Feature Engineering and Index Construction: To enhance the spectral signal related to soil salinity, this stage focused on feature engineering. A suite of novel salinity indices was systematically constructed using various mathematical transformations (addition, subtraction, multiplication, division, and power operations) on the extracted spectral reflectance data. The performance of these novel indices, along with existing ones, was evaluated by calculating the Pearson Correlation Coefficient between each index and the measured soil EC.

(c) Model Development and Optimization: A Stacking ensemble learning model was constructed to predict soil salinity. The first level of the model employed three

heterogeneous base learners—XGBoost, RF, and MLP—to capture diverse data features. The second level utilized a PLSR model as a meta-learner to integrate the predictions from the base models. The Optuna framework was employed for automated hyperparameter optimization to ensure the final model achieved maximum predictive accuracy and generalization capability.

(d) Model Application and Spatial Mapping: The fully trained and optimized Stacking model was applied to the entire Sentinel-2 dataset for the study area to perform a comprehensive and fine-grained inversion of soil salinity content. The resulting raster data, combined with the study area's vector boundary, was used within a Geographic Information System (GIS) environment to produce a high-resolution spatial distribution map of soil salinity.

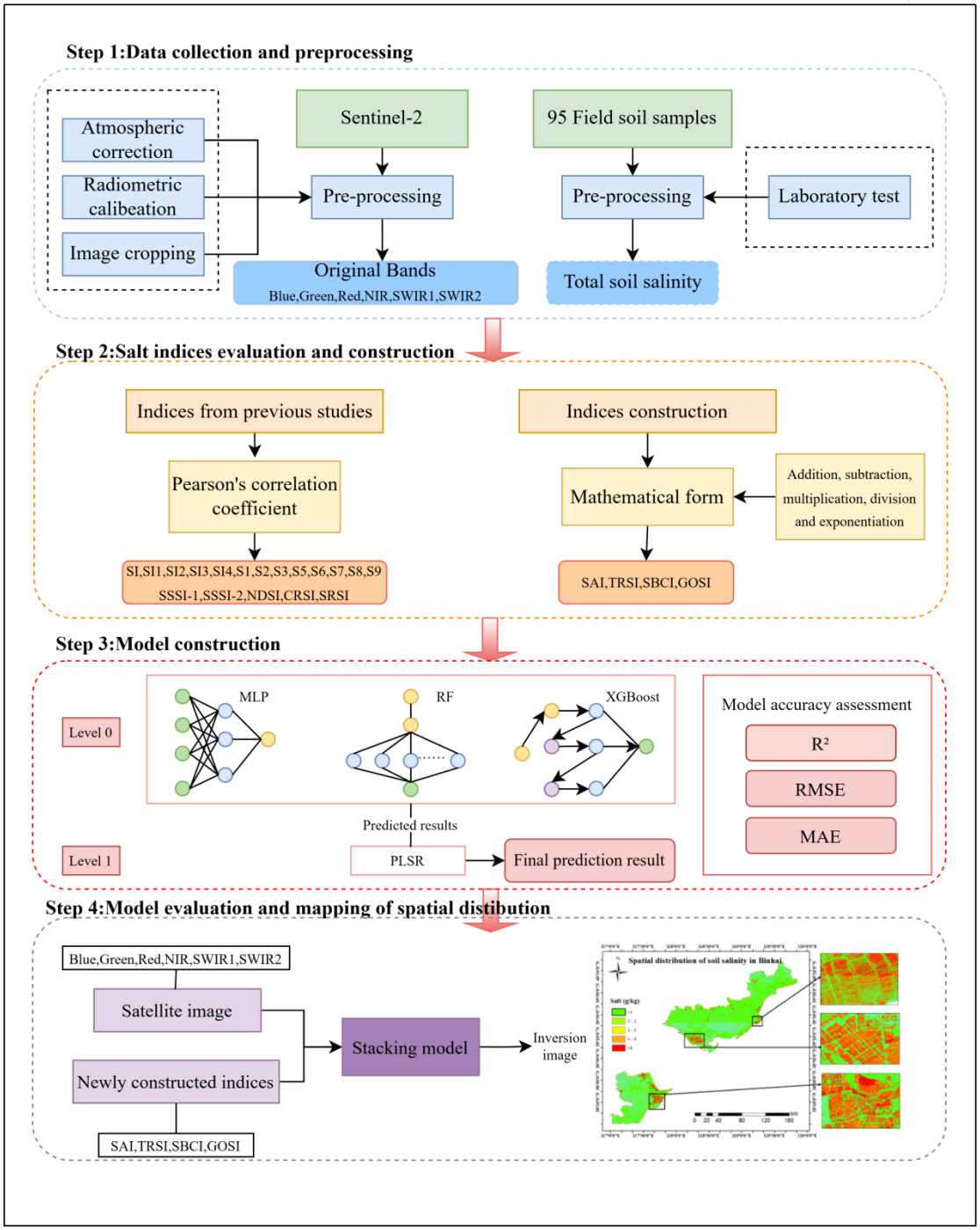


Figure 2: Methodological flowchart for soil salinity inversion.

## 2. Spectral Index Construction and Selection

### 2.1 Existing Salinity Indices

The spectral response of soil to varying salt content, particularly the general increase in reflectance across the visible to near-infrared spectrum with rising salinity, forms the physical basis for remote sensing-based monitoring(Peng et al., 2016). To establish a comprehensive baseline for comparison, this study systematically calculated and evaluated

17 widely recognized soil salinity indices from existing literature. These indices, listed in Table 2, represent a range of formulations developed for different sensors and environmental contexts(Wang et al., 2022).

Table 2: The existing salinity indices along with their explanation, abbreviations, formulas and reference.

| Explanation | Abbreviations | Formulations | Reference |
|---|---|---|---|
| Salinity index | SI | $(G \times R)^{0.5}$ | (Wang et al., 2013) |
| Salinity index 1 | SI1 | $(G + R)^{0.5}$ | (Khan et al., 2005) |
| Salinity index 2 | SI2 | $(NIR^2 + G^2 + R^2)^{0.5}$ | (Khan et al., 2005) |
| Salinity index 3 | SI3 | $(G^2 + R^2)^{0.5}$ | (Khan et al., 2005) |
| Salinity index 4 | SI4 | $SWIR_1 / NIR$ | (Douaoui et al., 2006) |
| Salinity index **I** | S1 | $B / R$ | (Khan et al., 2005) |
| Salinity index **II** | S2 | $(B - R)/(B + R)$ | (Khan et al., 2005) |
| Salinity index **III** | S3 | $G \times R / B$ | (Khan et al., 2005)) |
| Salinity index **V** | S5 | $B \times R / G$ | (Khan et al., 2005) |
| Salinity index **VI** | S6 | $R \times NIR / G$ | (Khan et al., 2005) |
| Salinity index **VIII** | S8 | $(G + R) / 2$ | (Douaoui et al., 2006) |
| Salinity index **IX** | S9 | $(G + R + NIR) / 2$ | (Douaoui et al., 2006) |
| Soil Salinity and Sodicity Indices1 | SSSI-1 | $R - NIR$ | (Bannari et al., 2008) |
| Soil Salinity and Sodicity Indices2 | SSSI-2 | $(R \times NIR - NIR^2) / R$ | (Bannari et al., 2008) |
| Normalized Difference | NDSI | $(NIR - SWIR_1)/(NIR + SWIR_1)$ | (MAJOR et al., 1990) |
| Salinity Index Canopy | CRSI | $[(NIR \times R - G \times B)/(NIR \times R + G \times B)]^{0.5}$ | (Scudiero et al., 2014) |
| Salinization Remote Sensing Index | SRSI | $[(NDVI - 1)^2 + SI^2]^{0.5}$ | (Alhammadi & Glenn, 2008) |

**2.2 Development of Novel Salinity Indices**

Recognizing that existing salinity indices often lack the specificity required for the complex coastal environment of the study area, a principled feature engineering approach was

undertaken to develop novel salinity indices tailored to local conditions. This process involved creating complex mathematical combinations of the six selected Sentinel-2 bands (B2, B3, B4, B8, B11, B12) to enhance the spectral signal associated with salinity while suppressing background noise from soil moisture, texture, and vegetation. Four novel three-band soil salinity indices were constructed: the Salt-Acuity Index (SAI), the Three-band Residual Soil Salinity Index (TRSI), the Salinity Brightness Correction Index (SBCI), and the Generalized Orthogonal Salinity Index (GOSI). These novel indices integrate complementary information from multiple bands to provide more predictive input features for subsequent machine learning models, thereby laying a solid foundation for high-accuracy soil salinity inversion.

Table 3: Novel Salinity Indices along with their explanation, abbreviations and formulas.

| Explanation | Abbreviations | Formulations |
|---|---|---|
| Salt-Acuity Index | SAI | $(G^2 - NIR^2 + SWIR_1^2)/(G \times NIR \times SWIR_1)$ |
| Three-band Residual Soil Salinity Index | TRSI | $(SWIR_1 - NIR + B)/(SWIR_1 + NIR - B)$ |
| Salinity Brightness Correction Index | SBCI | $SWIR_1/(R^2 + G^2)^{0.5}$ |
| Generalized Orthogonal Salinity Index | GOSI | $R - 0.5 \times NIR - 0.5 \times SWIR_1$ |

The performance of these novel salinity indices was systematically evaluated using Pearson correlation analysis to quantify the linear relationship between each index and the field-measured soil EC values(Wang et al., 2019).

**3. Stacking Ensemble Model Architecture**

In order to fully exploit the predictive ability of selected indices and improve the generalization ability and robustness of the model, this study adopted Stacking ensemble learning strategy. Stacking is a type of ensemble method which uses a meta-learner to learn the right combination of predictions from multiple base learners, instead of merely averaging or voting (Arvind Dagur et al. 2023). Stacking learning method can combine the advantages of different models and make up for the deficiencies of each model, which will improve the prediction accuracy (Zhan et al. 2025).

The Stacking model built in this study includes two levels in total: The first level (Level 0) is the base learner, including three models: mult-layer perceptron (MLP), random forest (RF) and extreme gradient boosting (XGBoost) (Pai et al. 2021). The second level (Level 1)is the meta-learner, and partial least squares regression (PLSR) model is used.

Level 0: MLP is a kind of typical feedforward neural network. It can learn and model the

complex and nonlinear relationship between input variables (spectral indices) and output variable (soil salinity) (Qi et al. 2022). RF is a kind of robust ensemble algorithm based on decision trees. By constructing a multitude of decorrelated decision trees to be trained on bootstrapped samples of the data and random subsets of features, the variance of the model can be greatly reduced and the problem of overfitting can be avoided. In addition, this algorithm is not sensitive to noisy and outlier data (Fernández-Delgado et al. 2014). XGBoost is a more efficient and more scalable implementation of gradient boosting decision trees (GBDT). XGBoost builds trees in a sequential fashion, with each new tree attempting to correct for the residuals of the previous tree. Second-order Taylor expansions, regularization, and parallelization strategies make this algorithm extremely successful in a variety of prediction tasks (Ye et al. 2022).

Level 1: PLSR is an efficient method in dealing with highly multicollinear predictors, and it is feasible to combine the predictors which may be correlated with the output variable well (Sihag et al. 2019). The predictors used by PLSR model in this study are the predictions extracted from the training datasets of the three base learners after five-fold cross-validation. The main task of the meta-learner is to learn the optimal weights to apply to the predictions of each base model, and finally output a more accurate and robust prediction. This two-level architecture enables the model to make full use of the nonlinear modeling ability of MLP, the anti-overfitting ability of RF and the high prediction accuracy of XGBoost, and build a powerful integrated model.

**4. Model Validation and Performance Evaluation**

To comprehensively assess model performance, the dataset of 95 samples was partitioned into a training set and a testing set. Three standard statistical metrics were selected for evaluation: the coefficient of determination (R2) Eq.(1), root mean square error (RMSE) Eq.**(2)**, and mean absolute error (MAE) Eq.**(3)**(Wang et al., 2023). The formulas for these metrics are as follows:

$$R^2=1-\frac{\sum_{i=1}^{n}(Z_i-\overline{Y})^2}{\sum_{i=1}^{n}(Z_i-\overline{Y})^2} \quad (1)$$

$$RMSE=\sqrt{\frac{\sum_{i=i}^{n}(Y_i-Z_i)^2}{n}} \quad (2)$$

$$MAE=\frac{\sum_{i=1}^{n}|Y_i-Z_i|}{n} \quad (3)$$

Where $Y_i$ is the measured value, $\overline{Y}$ is the mean of the measured values, $Z_i$ is the predicted value, and n is the number of samples.

**Results**

**1. Development and Performance of Novel Salinity Indices**

To overcome the limitations of existing salinity indices in complex surface environments, this study developed four novel salinity indices based on a deep analysis of the spectral response characteristics of soils with varying salt concentrations. The design of these indices was guided by the spectral curves shown in Figure 3, which reveal that increasing salinity not only causes an overall rise in reflectance across all bands (Figure 3a) but also introduces unique non-linear features and morphological changes when the spectra are subjected to mathematical transformations such as reciprocal (b), square (c), and square root (d) operations. These transformations highlighted latent patterns in inter-band response differences; for instance, the squaring operation amplified the signal in strongly reflecting bands, while the square root operation smoothed the data distribution. These observations inspired the design of indices capable of capturing the complex salt-spectrum relationship more effectively.

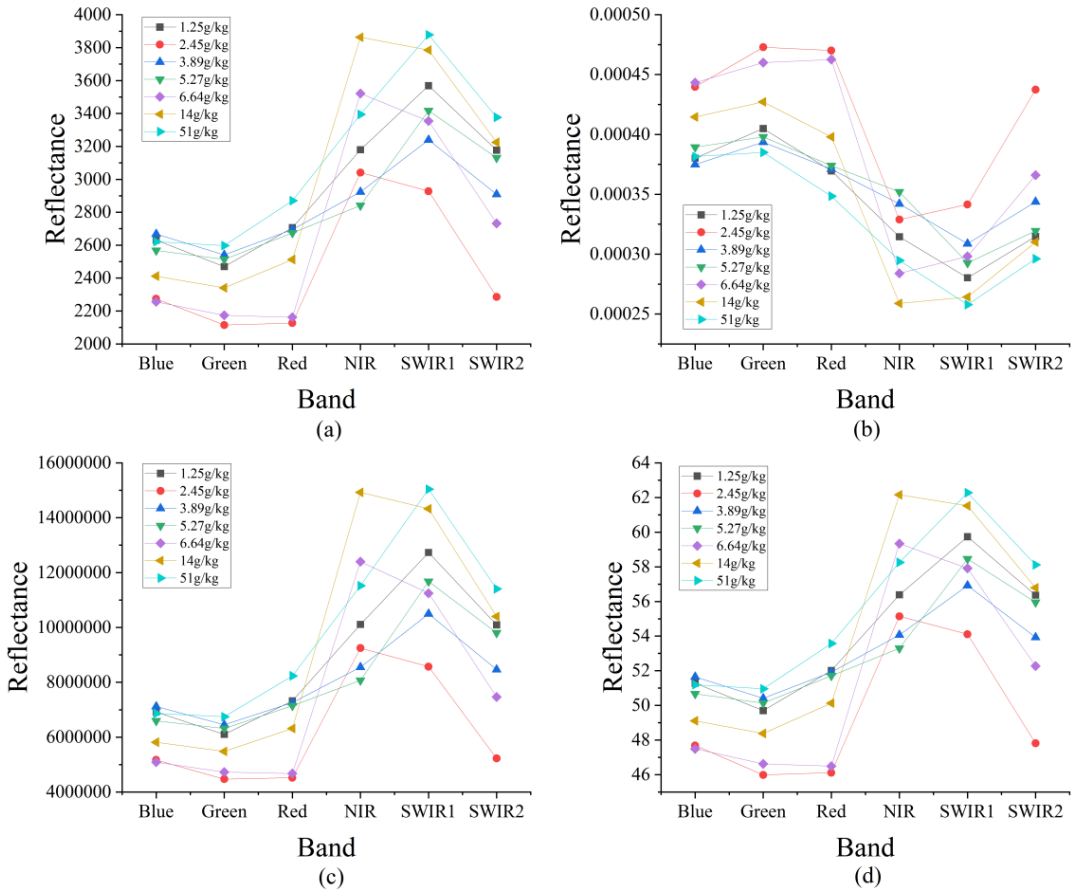

Figure 3: Spectral reflectance curves.

The four novel salinity indices were designed with specific physical rationales:

Salt-Acuity Index (SAI): This index employs a non-linear structure inspired by the observation that a squaring transformation can sharpen and amplify the subtle differences between the Green (G), Near-Infrared (NIR), and Short-Wave Infrared 1 (SWIR 1) bands caused by salinity, thereby increasing the detection "acuity" for salt stress.

Of course. Here is a description for the fourth index, following the format of the previous three.

Three-band Residual Soil Salinity Index (TRSI): This index is built on a residual concept, positing that the blue band (B) can serve as a stable baseline representing soil background reflectance with minimal influence from salinity or moisture. The core of the index, the difference between the SWIR 1 and NIR bands, captures the primary spectral response to soil salinity and moisture content. By adding the Blue band in the numerator and subtracting it in the denominator, the TRSI effectively calculates the "residual" signal after accounting for the baseline soil properties. This structure is designed to enhance sensitivity to salinity-induced changes while normalizing for variations in soil type, thus isolating the salinity signature more effectively.

Salinity Brightness Correction Index (SBCI): This index uses the Euclidean norm of the Red (R) and Green (G) bands to represent overall soil brightness. By normalizing the SWIR 1 band, which is sensitive to both salt and moisture, with this brightness factor, the SBCI effectively corrects for brightness variations caused by non-salinity factors like soil texture and color, thus isolating the salinity signal.

Generalized Orthogonal Salinity Index (GOSI): The linear combination form of this index is inspired by the orthogonalization concept used in vegetation indices. Its coefficients are structured to make the index approximately orthogonal to the primary axis of vegetation pixels in the spectral feature space, thereby minimizing interference from vegetation signals and ensuring high robustness in areas with varying vegetation cover.


Figure 4: Pearson correlation analysis results.

As shown in the Pearson correlation analysis (Figure 4), the four novel three-band indices—SAI (r=0.590), TRSI (r=0.608), SBCI (r=−0.462), and GOSI (r=0.486)—all demonstrated performance significantly superior to that of the existing salinity indices. The correlation coefficients of the novel indices with soil salt content were all higher than the maximum value observed among the 17 existing salinity indices and the 6 original spectral bands (r=0.414), with the highest correlation reaching 0.608. While a simple linear correlation cannot fully capture the complexity of soil salinity, this result provides strong evidence for the effectiveness of the feature engineering approach. It confirms that these novel indices can more accurately capture the spectral response characteristics of saline-alkali soils in this coastal region, providing a higher quality and more robust set of input features for the subsequent machine learning models.

**2. Comparative Evaluation of Predictive Models**

The performance evaluation results for five different predictive models (Stacking, XGBoost, RF, MLP, and PLSR), built using both the novel salinity indices (N-SI) and the existing indices (SI), are detailed in Table 4. An analysis of the key metrics—coefficient of

determination ($R^2$), root mean square error (RMSE), and mean absolute error (MAE) for both the calibration and validation sets—yields several key conclusions.

First, the application of the novel salinity indices led to a significant and consistent improvement in the predictive performance of all models. A direct comparison between the two sets of experiments reveals that, for both ensemble and single models, using the novel salinity indices as input features resulted in universally higher validation $R_v^2$ values and substantially lower $RMSE_v$ values. For example, the top-performing Stacking model achieved a validation $R_v^2$ of 0.870 with the novel indices, a marked increase from its 0.743 $R_v^2$ with the existing indices. Concurrently, its validation $RMSE_v$ dropped from 9.035 to 8.407. This demonstrates that the novel salinity indices provide more effective and representative information, enabling the models to make more accurate predictions with greater stability and generalization capability.

Second, among all the models tested, the Stacking ensemble learning model exhibited the most superior performance. When combined with the novel salinity indices, the Stacking model's evaluation metrics were optimal across the board. It achieved the highest calibration $R_c^2$ (0.928) and validation $R_v^2$ (0.870). It also recorded the lowest validation $RMSE_v$ (8.407) and $MAE_v$ (6.480). Compared to high-performing single models like XGBoost and RF, the Stacking model effectively fused the advantages of its diverse base learners, overcoming the limitations of any single model and achieving a breakthrough in both prediction accuracy and model robustness.

Table 4: Model evaluation.

| Metal | Method | $R_c^2$ | $RMSE_c$ | $MAE_c$ | $R_v^2$ | $RMSE_v$ | $MAE_v$ |
|---|---|---|---|---|---|---|---|
| N-SI | **Stacking** | **0.928** | **5.078** | **3.799** | **0.870** | **8.407** | **6.480** |
| | XGBoost | 0.897 | 6.375 | 3.279 | 0.768 | 8.815 | 9.611 |
| | RF | 0.784 | 9.485 | 5.796 | 0.773 | 9.260 | 7.641 |
| | MLP | 0.836 | 7.673 | 4.213 | 0.744 | 11.816 | 8.943 |
| | PLSR | 0.530 | 12.896 | 8.103 | 0.526 | 16.399 | 10.252 |
| SI | **Stacking** | **0.862** | **7.572** | **4.141** | **0.748** | **9.035** | **5.280** |
| | XGBoost | 0.847 | 7.986 | 5.000 | 0.702 | 9.643 | 7.107 |
| | RF | 0.902 | 6.066 | 3.067 | 0.728 | 11.499 | 6.586 |
| | MLP | 0.839 | 7.606 | 4.254 | 0.721 | 12.313 | 8.944 |
| | PLSR | 0.414 | 15.299 | 9.865 | 0.412 | 17.872 | 9.849 |

### 3. Analysis of Prediction Accuracy and Generalization

Figure 5 presents scatter plots of the predicted versus measured soil salinity values for the five models. The results provide a visual confirmation of the metrics in Table 4. For the Stacking model, the data points for both the training and testing sets are tightly clustered around the 1:1 reference line. This indicates an excellent fit during the training phase and, more importantly, a stable and accurate predictive performance on new data, demonstrating superior generalization ability. In contrast, while the RF and XGBoost models show a good fit on the training set, their testing set data points exhibit more significant deviation from the 1:1 line, particularly in the high-salinity range. This suggests a degree of overfitting and an insufficient capacity to predict high salinity values accurately. The data points for the MLP and PLSR models are much more dispersed for both training and testing sets, indicating that their goodness-of-fit and predictive accuracy are markedly inferior to the Stacking model. This comparative analysis further substantiates the superior performance of the Stacking ensemble model for soil salinity inversion.

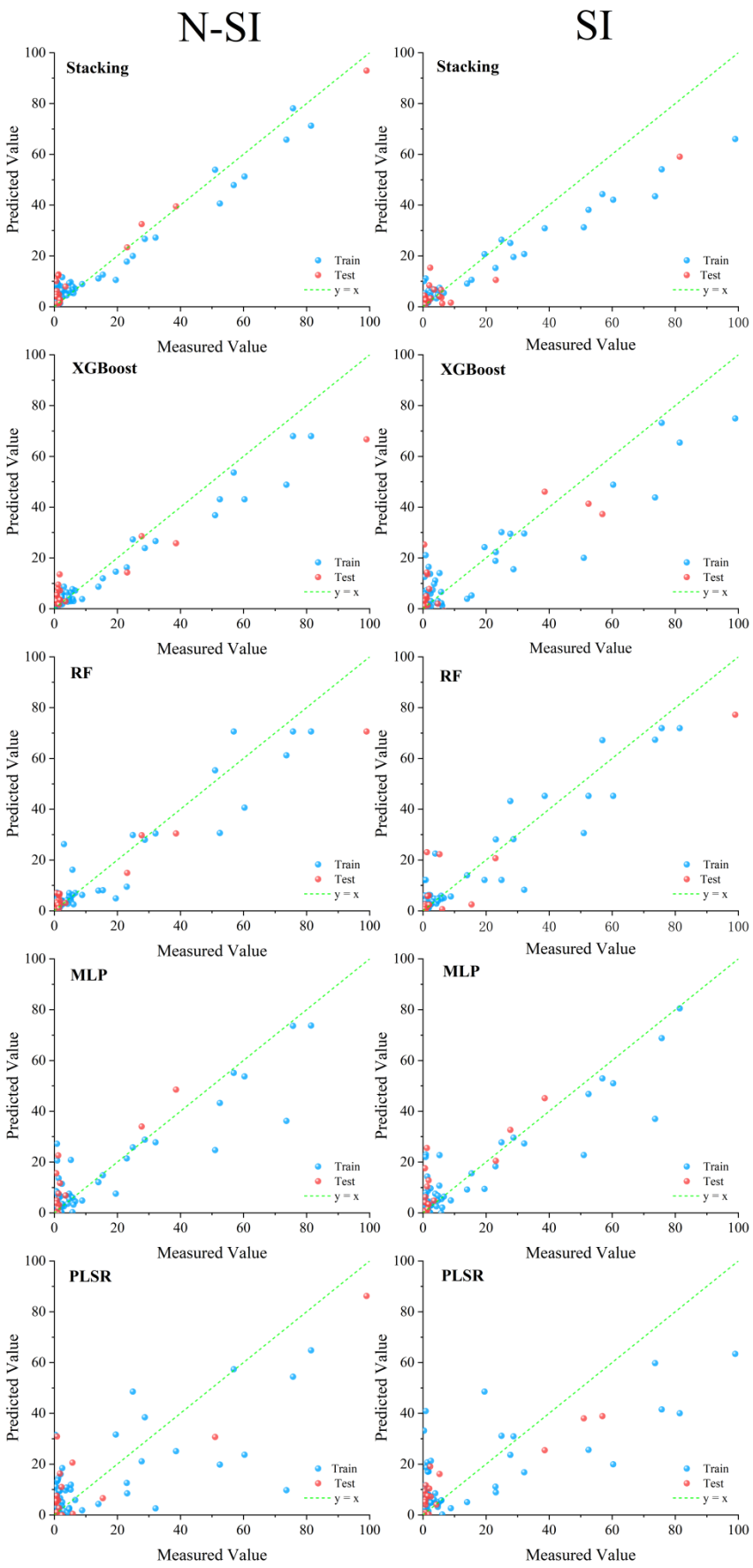


Figure 5: Scatter plots of predicted vs. measured soil salinity.

## 4. Spatial Mapping of Soil Salinity

Using the trained Stacking model, a high-resolution spatial distribution map of soil salinity was generated for the entire study area, clearly revealing the spatial heterogeneity of soil salt content (Figure 6). The classification of salinity levels is based on the standards from the Third National Soil Census of China (Table 5).

Table 5: Classification and Grading Standards for Soil Salinity in the Third National Soil Census.

| Region | Soil Salinity Type | | Indicator | Saline-Alkali Farmland | | | |
|---|---|---|---|---|---|---|---|
| | Cations | Anions | | Mild | Moderate | Severe | Solonchak / Solonetz |
| China Coastal Areas | Alkalinity < 5% | Chloride-dominated | Topsoil salt content (0-20cm) (g/kg) | 1~2 | 2~4 | 4~6 | >6 |

At a macro scale, the soil salinity distribution exhibits a distinct geographical differentiation. The majority of the area, particularly in the inland and western parts, is dominated by dark and light green colors, corresponding to "normal" (<1 g/kg) and "mildly saline" (1–2 g/kg) levels. This indicates a relatively healthy soil environment suitable for agriculture across most of the region. In stark contrast, soil salinity levels show a clear increasing gradient from the inland areas towards the coast. This trend is most pronounced in the northeastern coastal zone, where large expanses of yellow, orange, and red are concentrated, corresponding to "moderately saline" (2–4 g/kg), "severely saline" (4–6 g/kg), and "salt earth" (>6 g/kg) classes, respectively. This pattern is a classic representation of coastal soil salinization driven by the interplay of marine and terrestrial environmental factors.

To further validate the model's accuracy and spatial resolution, three typical high-salinity areas were magnified for detailed analysis. These areas are accurately identified as high-salinity zones on the inversion map, dominated by red and orange colors. Ground-truth information confirms that these three locations are artificial salt pans, a land-use type dominated by human activity. The model's successful identification of these known high-salinity features provides strong qualitative validation of its ability to capture fine-scale surface characteristics. Furthermore, the magnified images are not uniformly red but exhibit a mosaic or checkerboard pattern of red, orange, and even yellow and green. This internal heterogeneity indicates that the model can not only identify the overall high-salinity zone

but can also distinguish between different functional areas within the salt pans (e.g., high-concentration evaporation ponds versus lower-salinity dikes or channels), highlighting its high spatial resolution and sensitivity to subtle surface differences. This analysis demonstrates the model's capacity to effectively differentiate between diffuse salinization caused by natural processes (the coastal gradient) and concentrated salinization resulting from specific human land use (the salt pans), a distinction that is crucial for developing targeted and effective management strategies.

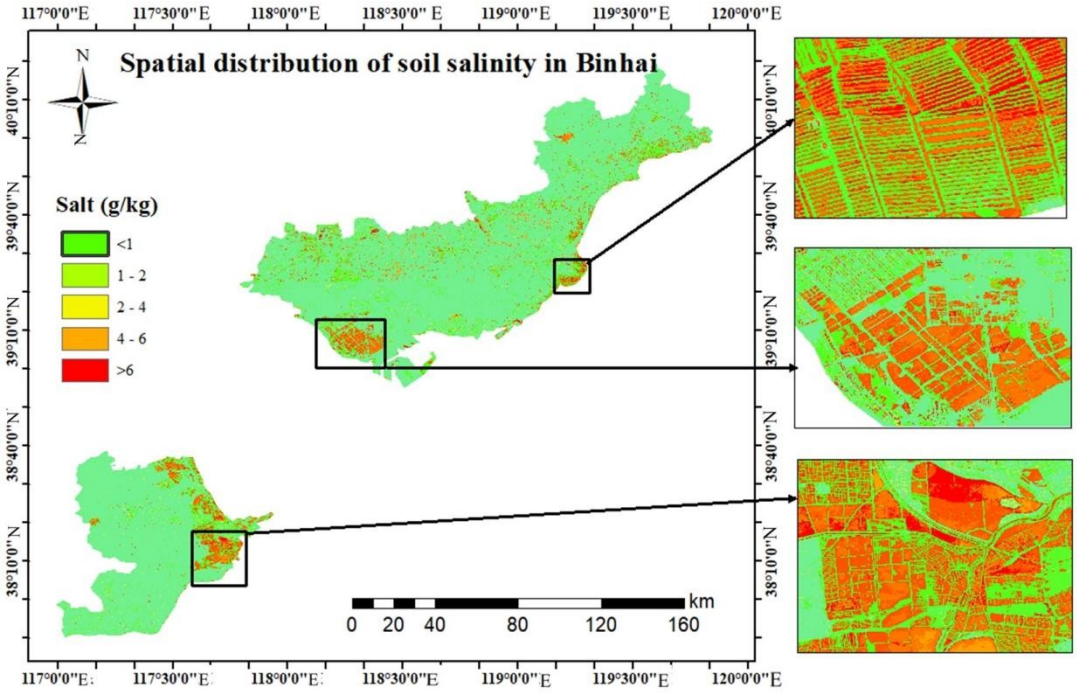


Figure 6: Soil salinity inversion map.

**Discussion and Conclusion**

This study successfully developed and validated a high-accuracy soil salinity inversion methodology based on a synergistic combination of novel salinity indices and a Stacking ensemble model, providing an effective framework for monitoring salinization using Sentinel-2 multispectral data.

The core innovation of this research first lies in the efficacy of the feature engineering process. The novel salinity indices, such as TRSI and SBCI, were designed through complex non-linear combinations of spectral bands to more sensitively capture the composite spectral response of soil salinity. The superior correlation of these indices with ground-truth EC values confirms that meticulous, physically-informed feature engineering can extract more predictive, deep information from existing remote sensing data compared to

traditional single-band or simple ratio indices. This step was crucial for enhancing the model's sensitivity to soil salinity.

Second, this research validates the exceptional performance of the Stacking ensemble model in handling complex geospatial data. The success of the model (R2=0.87) stems from its inherent collaborative effect. The heterogeneous base learners each contributed unique strengths: tree-based models like Random Forest and XGBoost efficiently handled non-linear relationships and demonstrated high robustness, while the Multilayer Perceptron excelled at learning deep, abstract patterns. By employing a two-level learning structure, the Stacking model integrated these diverse advantages, effectively mitigating the risk of any single model settling into a local optimum. The result was a final prediction that was more accurate and robust than any of its individual components, a finding consistent with previous research and which underscores the vast potential of ensemble learning in remote sensing inversion applications.

From a geographical process perspective, the soil salinity map generated in this study clearly reveals the spatial differentiation of salinization drivers in the region. At the macro scale, the distinct gradient of increasing salt content from inland areas toward the coast, peaking near estuaries, is primarily shaped by natural factors. These include tidal intrusion, seawater backflow, and the continuous upward migration of deep-soil salts to the surface via capillary action under high evaporation rates. At the micro-scale, the precisely identified "hotspots" corresponding to salt pans unequivocally point to the dominant role of anthropogenic activities in local salinization processes. Large-scale salt production industries, coupled with potentially irrational irrigation and drainage practices, have profoundly altered the local water-salt balance, creating highly saline artificial ecosystems. The model's ability to distinguish between these natural and human-induced salinization patterns is a significant achievement, providing critical spatial intelligence for land managers to prioritize and tailor interventions.

In conclusion, this study presents a novel and effective technical methodology for high-accuracy soil salinity monitoring. The framework, which combines innovative salinity indices with an advanced Stacking ensemble model, significantly improves prediction accuracy (R2=0.87) over conventional approaches. The resulting high-resolution map provides not only a valuable scientific basis for understanding the interplay between natural processes and human activities in the China Coastal Areas but also an actionable tool for precision agriculture and sustainable land management. Future research could build upon this work by integrating multi-source data (e.g., topography, climate, vegetation) and

employing geostatistical methods to quantitatively parse the contributions of different environmental factors to soil salinity variation. The robust and scalable nature of this methodology suggests its high potential for transferability to other coastal environments facing similar salinization challenges globally.

**Funding**

This research was supported by the Graduate Student Innovation Grant Program of North China Institute of Aerospace Engineering (YKY-2025-139).

**References**

Abbas, A., & Khan, S. (2007, January 1). *Using remote sensing techniques for appraisal of irrigated soil salinity*. International Congress on Modelling and Simulation (MODSIM). https://www.researchgate.net/publication/237421639_Using_Remote_Sensing_Techniques_for_Appraisal_of_Irrigated_Soil_Salinity

Alhammadi, M. S., & Glenn, E. P. (2008). Detecting date palm trees health and vegetation greenness change on the eastern coast of the united arab emirates using SAVI. *International Journal of Remote Sensing*, *29*(6), 1745–1765. https://doi.org/10.1080/01431160701395195

Arvind Dagur, Singh, K., Pawan Singh Mehra, & Dhirendra Kumar Shukla. (2023). Artificial intelligence, blockchain, computing and security volume 2. In *CRC Press eBooks*. Informa. https://doi.org/10.1201/9781032684994

Bannari, A., Guedon, A. M., El-Harti, A., Cherkaoui, F. Z., & El-Ghmari, A. (2008). Characterization of Slightly and Moderately Saline and Sodic Soils in Irrigated Agricultural Land using Simulated Data of Advanced Land Imaging (EO-1) Sensor. *Communications in Soil Science and Plant Analysis*, *39*(19-20), 2795–2811. https://doi.org/10.1080/00103620802432717

Boudibi, S., Sakaa, B., Benguega, Z., Fadlaoui, H., Othman, T., & Bouzidi, N. (2021). Spatial prediction and modeling of soil salinity using simple cokriging, artificial neural networks, and support vector machines in el outaya plain, biskra, southeastern algeria. *Acta Geochimica*, *40*(3), 390–408. https://doi.org/10.1007/s11631-020-00444-0

Davis, E., Wang, C., & Dow, K. (2019). Comparing sentinel-2 MSI and landsat 8 OLI in soil salinity detection: A case study of agricultural lands in coastal north carolina. *International Journal of Remote Sensing*, *40*(16), 6134–6153. https://doi.org/10.1080/01431161.2019.1587205

Dehni, A., & Lounis, M. (2012). Remote sensing techniques for salt affected soil mapping: Application to the oran region of algeria. *Procedia Engineering*, *33*(33), 188–198. https://doi.org/10.1016/j.proeng.2012.01.1193

Dong, H., & Tian, F. (2024). Soil salinity inversion based on a stacking integrated learning algorithm. *Agriculture*, *14*(10), 1777–1777. https://doi.org/10.3390/agriculture14101777

Douaoui, A. E. K., Nicolas, H., & Walter, C. (2006). Detecting salinity hazards within a semiarid context by means of combining soil and remote-sensing data. *Geoderma*, *134*(1-2), 217–230. https://doi.org/10.1016/j.geoderma.2005.10.009

FAO. (2021). *FAO knowledge repository*. Fao.org. https://openknowledge.fao.org/handle/20.500.14283/cb7247en

Fathizad, H., Ali Hakimzadeh Ardakani, M., Sodaiezadeh, H., Kerry, R., & Taghizadeh-Mehrjardi, R. (2020). Investigation of the spatial and temporal variation of soil salinity using random forests in the central desert of iran. *Geoderma*, *365*(365), 114233. https://doi.org/10.1016/j.geoderma.2020.114233

Fernández-Delgado, M., Cernadas, E., Barro, S., Amorim, D., & Fernández-Delgado, A. (2014). Do we need hundreds of classifiers to solve real world classification problems? *Journal of Machine Learning Research*, *15*(15), 3133–3181.

Hu, J., Peng, J., Zhou, Y., Xu, D., Zhao, R., Jiang, Q., Fu, T., Wang, F., & Shi, Z. (2019). Quantitative Estimation of Soil Salinity Using UAV-Borne Hyperspectral and Satellite Multispectral Images. *Remote Sensing*, *11*(7), 736. https://doi.org/10.3390/rs11070736

Jia, P., Zhang, J., Liang, Y., Zhang, S., Jia, K., & Zhao, X. (2024). The inversion of arid-coastal cultivated soil salinity using explainable machine learning and Sentinel-2. *Ecological Indicators*, *166*(166), 112364–112364. https://doi.org/10.1016/j.ecolind.2024.112364

Khan, N. M., Rastoskuev, V. V., Sato, Y., & Shiozawa, S. (2005). Assessment of hydrosaline land degradation by using a simple approach of remote sensing indicators. *Agricultural Water Management*, *77*(1-3), 96–109. https://doi.org/10.1016/j.agwat.2004.09.038

Konstantin Ivushkin, Harm Bartholomeus, Bregt, A. K., & Alim Pulatov. (2016). Satellite thermography for soil salinity assessment of cropped areas in uzbekistan. *Land Degradation and Development*, *28*(3), 870–877. https://doi.org/10.1002/ldr.2670

Liang, Z., Wang, F., Zhu, J., Li, P., Xie, F., & Zhao, Y. (2024). Autonomous extraction technology for aquaculture ponds in complex geological environments based on multispectral feature fusion of medium-resolution remote sensing imagery. *Remote Sensing*, *16*(22), 4130–4130. https://doi.org/10.3390/rs16224130

Ma, H., Zhao, W., Duan, W., Ma, F., Li, C., & Li, Z. (2024). Inversion model of soil salinity in alfalfa covered farmland based on sensitive variable selection and machine learning algorithms. *PeerJ*, *12*(12), e18186–e18186. https://doi.org/10.7717/peerj.18186

MAJOR, D. J., BARET, F., & GUYOT, G. (1990). A ratio vegetation index adjusted for soil brightness. *International Journal of Remote Sensing*, *11*(5), 727–740. https://doi.org/10.1080/01431169008955053

Nguyen, K.-A., Liou, Y.-A., Tran, H.-P., Hoang, P.-P., & Nguyen, T.-H. (2020). Soil salinity assessment by using near-infrared channel and vegetation soil salinity index derived from landsat 8 OLI data: A case study in the tra vinh province, mekong delta, vietnam. *Progress in Earth and Planetary Science*, *7*(1). https://doi.org/10.1186/s40645-019-0311-0

Pai, K.-C., Wang, M.-S., Chen, Y.-F., Tseng, C.-H., Liu, P.-Y., Chen, L.-C., Sheu, R.-K., & Wu, C.-L. (2021). An artificial intelligence approach to bloodstream infections prediction. *Journal of Clinical Medicine*, *10*(13), 2901. https://doi.org/10.3390/jcm10132901

Peng, J., Ji, W., Ma, Z., Li, S., Shi, Z., & Zhou, L. (2016). Predicting total dissolved salts and soluble ion concentrations in agricultural soils using portable visible near-infrared and mid-infrared spectrometers. *Biosyst.Eng*, *152*(152), 94–103. https://doi.org/10.1016/j.biosystemseng.2016.04.015

Qi, S., He, M., Bai, Z., Ding, Z., Sandhu, P., Zhou, Y., Peyman Namadi, Tom, B., Hoang, R., & Anderson, J. (2022). Multi-Location emulation of a process-based salinity model using machine learning. *Water*, *14*(13), 2030–2030. https://doi.org/10.3390/w14132030

Sabyasachi Kabiraj, Marappan Jayanthi, Muthusamy Samynathan, & Selvasekar Thirumurthy. (2023). Automated delineation of salt-affected lands and their progress in coastal india using google earth engine and machine learning techniques. *Environmental Monitoring and Assessment*, *195*(3). https://doi.org/10.1007/s10661-023-11007-0

Scudiero, E., Skaggs, T. H., & Corwin, D. L. (2014). Regional scale soil salinity evaluation using landsat 7, western san joaquin valley, california, USA. *Geoderma Regional*, *2-3*(2-3), 82–90. https://doi.org/10.1016/j.geodrs.2014.10.004

Sihag, P., Keshavarzi, A., & Kumar, V. (2019). Comparison of different approaches for modeling of heavy metal estimations. *SN Applied Sciences*, *1*(7). https://doi.org/10.1007/s42452-019-0816-6

Wang, D., Yang, H., Qian, H., Gao, L., Li, C., Xin, J., Tan, Y., Wang, Y., & Li, Z. (2023). Minimizing vegetation influence on soil salinity mapping with novel bare soil pixels from multi-temporal images. *Geoderma*, *439*(439), 116697–116697. https://doi.org/10.1016/j.geoderma.2023.116697

Wang, F., Chen, X., Luo, G., Ding, J., & Chen, X. (2013). Detecting soil salinity with arid fraction integrated index and salinity index in feature space using landsat TM imagery. *Journal of Arid Land*, *5*(3), 340–353. https://doi.org/10.1007/s40333-013-0183-x

Wang, J., Peng, J., Li, H., Yin, C., Liu, W., Wang, T., & Zhang, H. (2021). Soil salinity mapping using machine learning algorithms with the sentinel-2 MSI in arid areas, china. *Remote Sensing*, *13*(2), 305–305. https://doi.org/10.3390/rs13020305

Wang, N., Peng, J., Chen, S., Huang, J., Li, H., Biswas, A., He, Y., & Shi, Z. (2022). Improving remote sensing of salinity on topsoil with crop residues using novel indices of optical and microwave bands. *Geoderma*, *422*(422), 115935–115935. https://doi.org/10.1016/j.geoderma.2022.115935

Wang, Y., Ding, J., Yu, D., Ma, X., Zhang, Z., Ge, X., Teng, D., Li, X., Liang, J., Lizaga, I., Chen, X., Yuan, L., & Guo, Y. (2019). Capability of Sentinel-2 MSI data for monitoring and mapping of soil salinity in dry and wet seasons in the Ebinur Lake region, Xinjiang, China. *Geoderma*, *353*(353), 172–187. https://doi.org/10.1016/j.geoderma.2019.06.040

Ye, M., Zhu, L., Li, X., Ke, Y., Huang, Y., Chen, B., Yu, H., Li, H., & Feng, H. (2022). Estimation of the soil arsenic concentration using a geographically weighted xgboost model based on hyperspectral data. *The Science of the Total Environment*, *858*(858), 159798–159798. https://doi.org/10.1016/j.scitotenv.2022.159798

Zarei, A., Hasanlou, M., & Mahdianpari, M. (2021). A comparison of machine learning models for soil salinity estimation using mult-spectral earth observation data. *ISPRS Annals of the Photogrammetry, Remote Sensing and Spatial Information Sciences*, *V-3-2021*(3), 257–263. https://doi.org/10.5194/isprs-annals-v-3-2021-257-2021

Zhan, D., Liu, Y., Yang, W., Lu, M., & Song, Y. (2025). Spatial variability of soil salinity in coastal saline-alkali farmlands: A novel approach integrating a stacked model with the reconstructed

in-situ hyperspectral feature. *Computers and Electronics in Agriculture*, *235*(235), 110376–110376. https://doi.org/10.1016/j.compag.2025.110376